UTILISATION OF COMPUTATIONAL FLUID DYNAMICS TECHNIQUES FOR DESIGN OF MOLYBDENUM TARGET SPECIFICATION

G. H. Yeoh and D. Wassink

Australian Nuclear Science and Technology Organisation (ANSTO), PMB 1, Menai, NSW 2234, Australia

Abstract

A three-dimensional computational fluid dynamics (CFD) model to investigate the hydraulic behaviour within a model of the liner and irradiation rig, located in the central portion of the HIFAR fuel element is described. Flow visualisation and LDV measurements are performed to better understand the fluid flow around the narrow spaces within the irradiation rig, annular target cans and liner. Based on the unstructured meshing consisted of triangular elements and tetrahedrons within the flow space generated for the geometrical structure, the CFD model was able to predict complex flow structures inside the liner containing the irradiation rig and target cans. The reliability of the model was validated against experiments. The predicted flow behaviour was comparable to the experimental observations. Predicted velocities were also found to be in good agreement with LDV measurements.

INTRODUCTION

Computational fluid dynamics (CFD) is a tool that is becoming increasing popular to study complex fluid flows. The use of CFD-based methodology has many advantages. It has the potential for reducing the extent and number of experiments required in describing flow structures and in some circumstances significantly more insights could be extracted regarding the flow behaviour. It can also assist in circumventing predictions of flows in complicated shape geometries where empirically derived relationships may not be confidently applied beyond the narrow range of geometries and operating conditions over which they were determined. In the nuclear industry, such possibilities are critical especially the need to understand the complex thermal-hydraulic flow and heat transfer phenomena that exist within the fuel element space where sealed target cans are placed for molybdenum production. It is therefore not surprising that the use of CFD-based methodology provides attractive benefits, as this approach can provide substantial insight into physical processes through the solutions of governing equations that are formulated from fundamental principals of fluid mechanics and heat transfer. These equations are usually iteratively solved for each discretised element in the physical space with robust and efficient solvers. Since large number of these discretised elements (thousands and in some circumstances millions) are usually required to resolve the physical processes within the computational domain, accurate predictions of the fluid flow parameters could be obtained.

In the quest of confidently employing the CFD-based methodology for nuclear applications, a prerequisite condition is validation of the developed models within the CFD computer program. This step is important to ensure that the full potential of the CFD models to be used for design considerations can be realised. Through the water tunnel facility at ANSTO, flow visualisations and measurements at discrete number of locations within the narrow spaces in the transparent mock-up irradiation rig model have been performed through a non-intrusive point velocity measurement made possible by the use Laser Doppler Velocimetry (LDV). These flow visualisations and measurements can substantially assist in checking the CFD model predictions of the fluid flow within the modified mock-up model.

We have recently employed a commercial CFD computer code CFX4 [1] to study the irradiation of a prototype LEUFR target can containing a small uranium metal foil in the reactor core of a High Flux Australian Reactor (HIFAR) fuel element. Modelling such process is challenging because of, the complicated geometry of the irradiation rig and target cans, having a wide spectrum of length scales, and the requirement to accurately model the heat transfer coupled to the fluid flow through multi-material solid regions. The approach has shown to provide substantial insights into the physical processes involving the simultaneous response of the fluid and heat flow. Significantly, model

predictions were found to yield good agreement with thermocouple measurements during the test irradiation experiments.

In this paper, we report work in progress directed towards a better understanding of the complex thermal-hydraulic behaviour in the irradiated HIFAR fuel element space where new designs of the target cans for molybdenum production are evaluated. Here, we further explore the possibility for the usage of this versatile tool to parametrically investigate the flow and heat transport behaviours for design change to another prototype of the LEUFR target can that encloses a larger uranium metal foil. The latest trend in CFD utilisation is the unstructured mesh approach to better accommodate complicated geometrical structures and we have employed CFX5 [2] in this present study. Work is still ongoing towards the final design specifications of the target can for full molybdenum production. Here, we present results of the preliminary CFD simulation of the fluid flow of this current design proposal of the target can modelled against the modified mock-up model in the water tunnel facility.

DESCRIPTION OF THE HIFAR FUEL ELEMENT

Figure 1 presents the schematic drawing of the existing fuel element in HIFAR [3]. Heavy water enters the fuel element through the "guide nose" and flows upwards. When the coolant reaches the liner, a small fraction of the heavy water enters the liner via four small holes on the liner nose cone. The remainder of the coolant flows through the fuel tubes The low velocity flow inside the liner moves up through a vertical space containing an irradiation rig and sealed target cans. Details of the design of the irradiation rig and placements of the targets within the rig are described in the next section. Water flowing over the surfaces of the target cans removes the fission heating produced. To effectively dissipate the large amount of heat generated during the irradiation process into the coolant, , the components that include the target cans, rig and liner are generally made of Aluminium

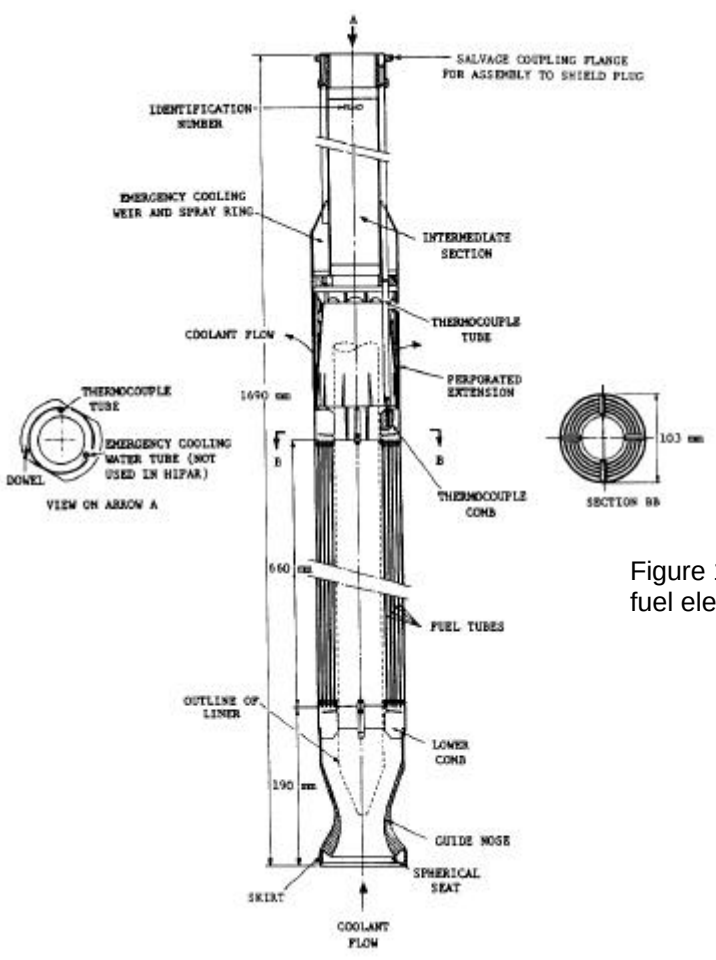

Figure 1. Schematic description of the HIFAR fuel element.

EXPERIMENTAL APPARATUS AND METHOD

Figure 2 describes the mock-up model of the prototype design of the irradiation rig and annular target cans that are placed in the water tunnel facility. The outside diameter of the liner is sealed to the test section so that the flow path is only through the liner inlet holes. An Endress and Hauser Promag flowmeter is used to measure the flow rates within the facility.

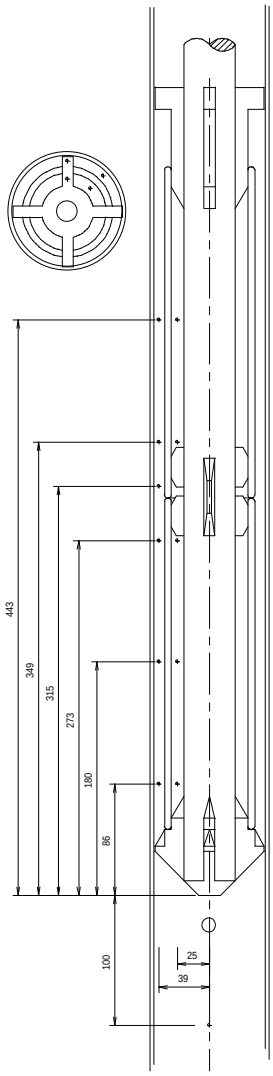

Figure 2. Schematic drawing of the X216 Rig 1.7:1 Scale Acrylic Model.

Flow visualisation of the fluid flow is performed using an Argon Ion laser light sheet, high-resolution digital camera and standard video equipment. The flow is seeded with Iriodin powder concentrations of 0.5 to 1 gram per 3000 litres of water. Hydrogen and Oxygen bubbles generated by electrolysis, are also used as flow tracers. Particles in the flow are illuminated while they are in the field of the laser light sheet. With the digital images and video footage the flow field is clearly visible.

Velocities are measured using a two-dimensional (2D) Dantec LDV system, operated in 1D mode measuring axial velocity components. Difficulties were encountered in measuring radial components due to refraction from the curved surfaces of the model. Data are stored on the computer attached to the LDV hardware. Uncertainty in measurement using the LDV equipment is determined to be a maximum of ± 3.5% for a particular optics configuration but generally less than ±1.8%. Points of velocity measurement are shown in Figure 2. Measurements are taken using the LDV probe both in forward scatter and backscatter mode, with verification between modes at a number of points.

CFD MODEL DESCRIPTION

Governing Equations

Simulations of the fluid flow are handled through solutions to strongly coupled filtered (time-averaged) conservation equations of mass and momentum formulated from fundamental principals of fluid

mechanics. Analytical solutions to these equations exist for only the simplest of flows under ideal conditions. To obtain solutions for real flows, a numerical approach must be adopted whereby the equations are replaced by algebraic approximations that may be solved using a numerical method. In order to achieve closure of the turbulent flow, the standard-equation κ-ε model is used. The model solves two-differential equations for the turbulent kinetic energy (κ) and its dissipation (ε).

Unstructured Meshing

The construction of the mock-up model for meshing is challenging because of the inherent intricate details of the irradiation rig and the placements of the annular targets within the rig. The mesh is prepared in two stages. A surface mesh of triangular mesh elements is initially generated on all the surfaces covering the model components. The volume mesh consists of tetrahedral elements is then subsequently inserted within the fluid flow domain from the surface mesh elements. Figure 3 shows the mesh layout of triangular surface elements around the pin and support tube nose cone of the irradiation rig. For the entire geometrical structure that includes the assembly of two annular target cans placed within the prototype rig in the liner and mock-up fuel element, a volume mesh of 605158 tetrahedrons and a surface mesh of 42030 triangular elements are allocated.

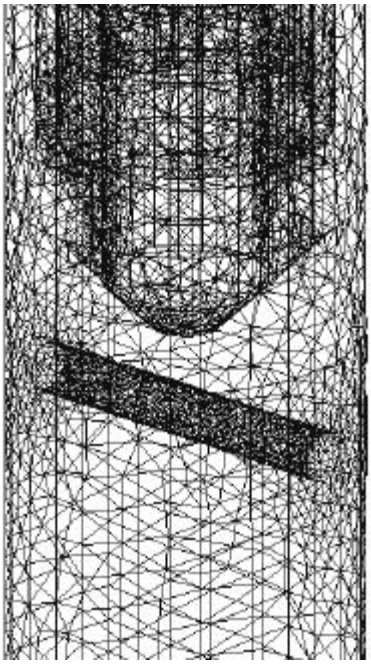

Figure 3. Surface triangular mesh distribution for the pin and support tube nose cone of the irradiation rig.

Boundary Conditions

The inlet normal velocity is determined through the experimental mass flow rate of 1.6965 kgs^{-1}. Turbulence kinetic energy κ and its dissipation rate ε are obtained from the following empirical relationships:

$$k = \frac{3}{2}\mathrm{I}^2\mathrm{U}^2 \quad ; \quad \mathrm{e} = \frac{k^{3/2}}{0.3\mathrm{D}_\mathrm{h}} \tag{1}$$

where *I* is the specified turbulence intensity, *U* is the inlet normal velocity and D_h is the hydraulic diameter of the inlet surface. At the outlet, mass flow boundaries are applied to conserve the mass of the flow system. No-slip condition is employed for the velocities on the solid wall surfaces. For the near-wall treatment of the viscosity affected sublayer region of the solid boundary, logarithmic wall functions are used to provide near wall boundary conditions for the mean flow and turbulence transport equations.

Computational Procedure

The governing equations to be solved by matrix solution techniques are formulated by integrating the system of equations using the finite volume method over small elemental volumes. For each elemental volume, the relevant quantity (mass, momentum and turbulence) is conserved in a discrete sense for each control volume.

CFX5 uses a coupled solver, which solves the hydrodynamic equations (for velocities and pressure) as a single system. It has been found in the segregated approach in CFX4 that the strategy to first solve the momentum equations using a guessed pressure and an equation for a pressure correction resulted in a large number of iterations to achieve reasonable convergence. By adopting the coupled solver, it has been established that such a coupled treatment significantly outweighs the segregated approach in terms of robustness, efficiency, generality and simplicity. To accelerate convergence for each of the discretised algebraic equations, CFX5 employs the Algebraic Multigrid solver [4].

The non-linear partial differential equations are marched to steady state. Convergence is deemed to have been reached with the normalised residual mass is less than 1.0×10^{-4}.

RESULTS AND DISCUSSION

CFD simulation of the fluid flow through the model of the irradiation rig and annular target cans was performed. Figure 4 illustrates the flow distribution inside and outside of the liner nose cone. Based on the experimental flow rate of 1.6965 kgs^{-1} and a base diameter of 0.3 m of the mock-up fuel element model, there existed a very low flow velocity outside of the liner nose cone as observed in Figure 4(b). Nevertheless, the fluid being directed through the small size bottom and side holes of the liner nose cone caused these merging flows to interact yielding a very highly complicated flow structure consisting of multiple vortices of recirculating flows (see Figure 4(a)). It was also evident that due to the significant acceleration of the flow found near the liner holes, the velocities increased dramatically to a magnitude of 5.0 ms^{-1} and resulted in large pressure drops. Near the bottom hole of the liner nose cone, the CFD model predicted a normal velocity of approximately of 3 ms^{-1}. This predicted value has been found to be in good agreement with experimental LDV measurement of 2.6 ms^{-1}, which provided confidence to the reliability of the models in the CFD computer program. As the fluid moved vertically upwards, the flow gradually became more uniform.

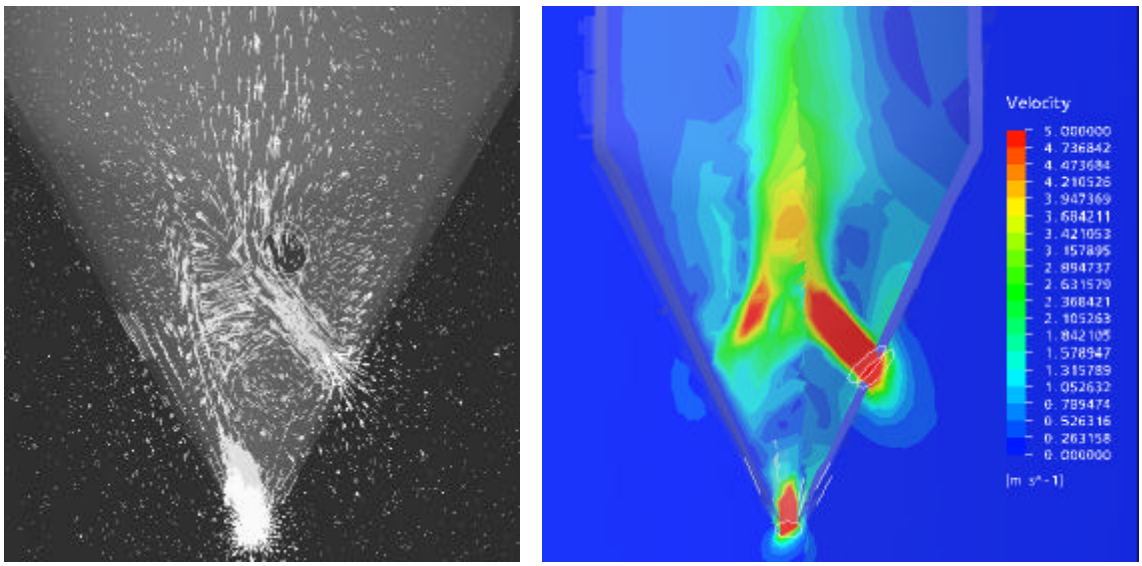

(a) (b)

Figure 4. Flow distribution inside and outside of the liner nose cone: (a) Velocity vectors and (b) Velocity contours.

Another important consideration for the molybdenum rig and target specification was the incorporation of a pin situated at some distance below the placement of the rig as can be seen in Figure 5. This design feature was considered and implemented in the liner because of safety concerns in the event of a possible accident where the rig may fall through to the bottom and impact on the liner nose cone.

The selection of pin size is an important requirement for the rig and target specification. From the flow predictions in Figure 5(a), it could be ascertained that the pin size chosen contributed to only minor flow disturbances in the area between the pin and the bottom surface of the rig nose cone. It was also observed that majority of the bulk fluid flow was unperturbed and diverged smoothly as it approached the rig. Flow visualisation performed during experiments (see Figure 5(b)) projected a similar flow pattern, which further confirmed the reliability of the CFD model predictions.

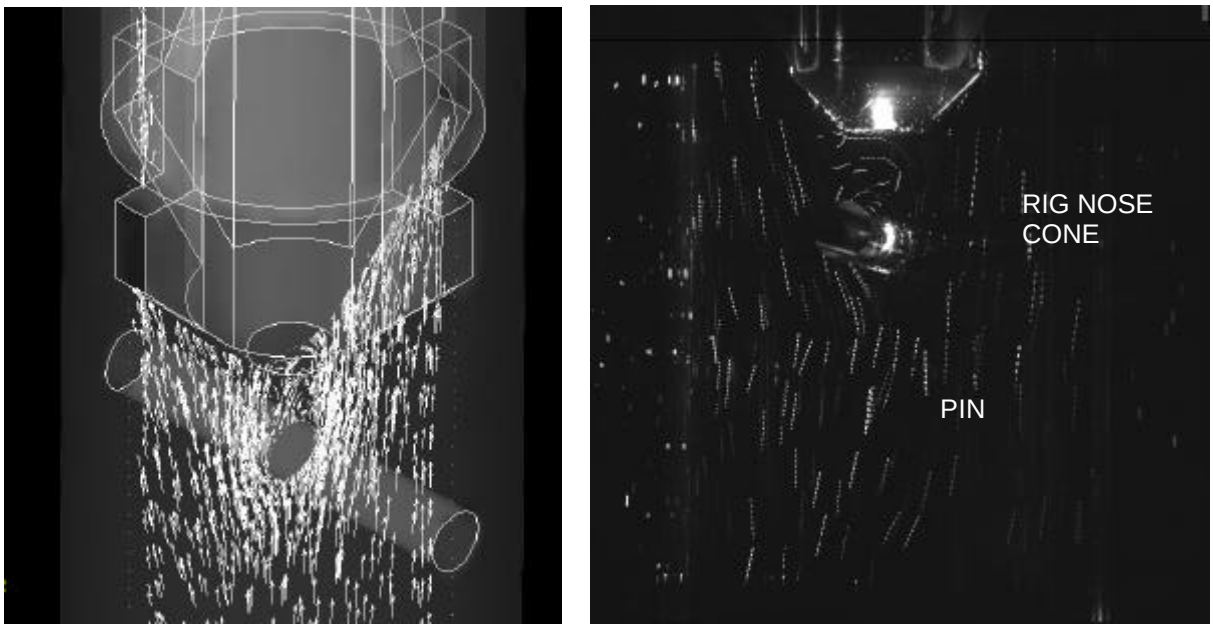

(a) (b)

Figure 5. Flow distribution around the pin situated some distance below the rig nose cone: (a) Predicted velocity vectors and (b) Streaklines in the experimental case.

Figure 6 presents the flow distribution of the fluid travelling between the inner annular can wall and rig outer surface designated for the purpose of illustration as region 1 and the area between the outer annular can wall and the liner inner surface designated as region 2. The fluid flowing within these spaces was found to be rather uniform. These favourable flow structures indicated that axial cooling along the length of the target could remove the heat effectively for the prototype can design where uranium foils are embedded in the sealed annular targets during the irradiation process for molybdenum production. An interesting aspect of the model predictions through the velocity contours in Figure 6(b) showed more fluid moving vertically upwards in region 2 than in region 1. Based on the LDV flow measurements at the discrete locations in regions 1 and 2 in Figure 2, the experiments confirmed the CFD predictions of the different velocities in the two regions. Velocity values of 0.44 ms^{-1} and 0.502 ms^{-1} were measured during experiments for regions 1 and 2 respectively. The predicted velocities as depicted by the velocity contours in Figure 6(b) are in good agreement with the experimental velocities.

CONCLUSION

Details of a three-dimensional CFD model to study the hydraulic behaviour within a model of a prototype irradiation rig and annular target cans have been described. An unstructured meshing consisted of triangular elements and tetrahedrons within the flow space for the geometrical structure was successfully created. Flow visualisation and LDV measurements were also performed to better understand the fluid flow around the narrow spaces within the irradiation rig, annular target cans and liner. The CFD model was capable of predicting complex flow structures inside the liner containing the irradiation rig and target cans. In regards to its reliability, the model results have shown to agree qualitatively with experimental observations and measurements.

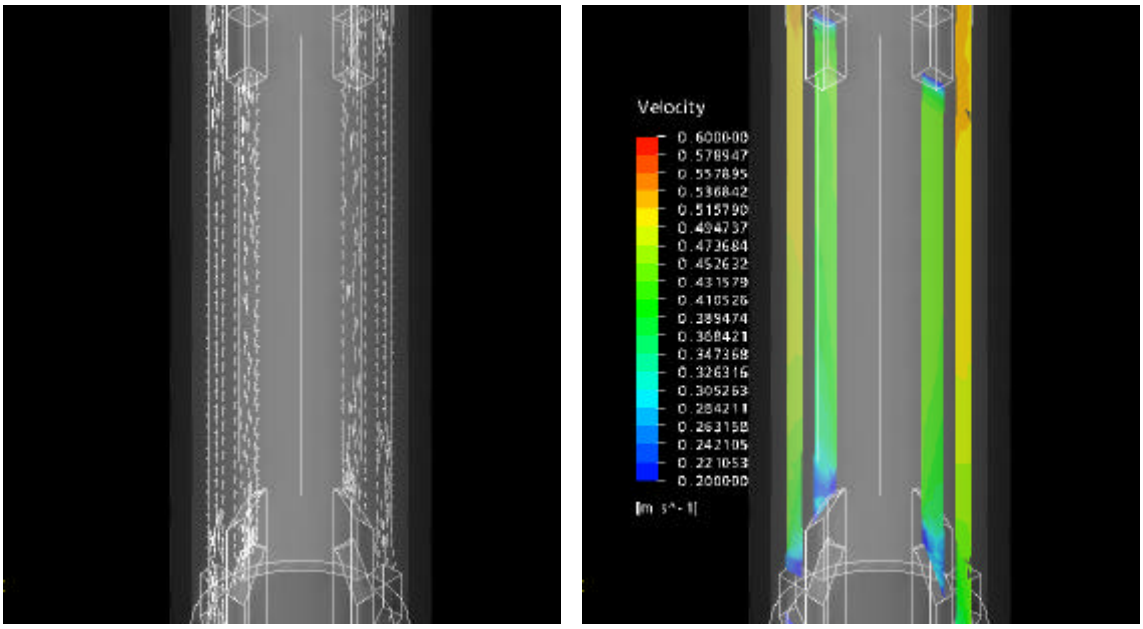

(a) (b)

Figure 6. Predicted flow distribution around the annular target can: (a) Velocity vectors and (b) Velocity contours

Acknowledgments

The authors gratefully acknowledge the support from Therese Donlevy and Peter Anderson of the Radiopharmaceutical division of ANSTO.

REFERENCES

[1] CFDS-AEA Technology, 2000, *CFX User's Guide*, Version 4.4.
[2] CFDS-AEA Technology, 2003, *CFX User's Guide*, Version 5.5.1.
[3] Australian Nuclear Science Technology Organisation (ANSTO), 1972, *HIFAR Descriptive Manual*, HIFAR Safety Document Section 3.
[4] Hutchision, B. R. and Raithby, G. D., 1986, "A Multigrid Method Based on the Additive Correction Strategy," *Num. Heat Transfer*, Vol. 9, pp. 511-537.